

SUZAKU VIEW OF THE SWIFT/BAT ACTIVE GALACTIC NUCLEI. IV. NATURE OF TWO NARROW-LINE RADIO GALAXIES (3C 403 AND IC 5063)

FUMIE TAZAKI¹, YOSHIHIRO UEDA¹, YUICHI TERASHIMA², AND RICHARD F. MUSHOTZKY³

Draft version June 16, 2011

ABSTRACT

We report the results of *Suzaku* broad band X-ray observations of the two narrow-line radio galaxies (NLRGs), 3C 403 and IC 5063. Combined with the *Swift*/BAT spectra averaged for 58 months, we are able to accurately constrain their spectral properties over the 0.5–200 keV band. The spectra of both nuclei are well represented with an absorbed cut-off power law, an absorbed reflection component from cold matter with an iron-K emission line, and an unabsorbed soft component, which gives a firm upper limit for the scattered emission. The reflection strength normalized to the averaged BAT flux is $R \equiv \Omega/2\pi \approx 0.6$ in both targets, implying that their tori have a sufficiently large solid angle to produce the reprocessed emission. A numerical torus model with an opening angle of $\sim 50^\circ$ well reproduces the observed spectra. We discuss the possibility that the amount of the normal gas responsible for Thomson scattering is systematically smaller in radio galaxies compared with Seyfert galaxies.

Subject headings: galaxies: active – galaxies: individual (3C 403, IC 5063) – X-rays: galaxies

1. INTRODUCTION

Modern astronomy has revealed that the mass of a super-massive black holes (SMBHs) in a galactic center has tight correlation with the mass of the bulge of the host galaxy (e.g., Magorrian et al. 1998; Marconi & Hunt 2003), indicating the co-evolution between SMBHs and galaxies. According to theoretical predictions, active galactic nuclei (AGNs) may play a key role in regulating both mass accretion and star formation by their feedback through powerful outflows and/or radiation to the surrounding gas (e.g., Di Matteo et al. 2005). Broadband X-ray observations of AGNs are particularly important to study the physics of accretion and outflow in the central engine by measuring the spectra and time variability of the continuum emission from the innermost disk and relativistic jets. They also provide unique information on the structure of the tori surrounding the accretion disk, which may be the source of mass accretion and site of nuclear starbursts (e.g., Davies et al. 2007; Imanishi & Wada 2004), through investigation of its reprocessed emission.

Recent hard X-ray all sky surveys above 10 keV conducted by *Swift*/BAT and *INTEGRAL* are providing us with an ideal sample of AGNs in the local universe that can be efficiently followed-up with observatories having a narrow field-of-view, like *Suzaku* and *XMM-Newton*, for detailed spectroscopic studies. *Suzaku* has unique features covering the wide energy band over 0.1–600 keV with good energy resolution and large collecting area below 10 keV. Making use of these capabilities, we have been working on a program of *Suzaku* follow-up observations of *Swift*/BAT AGNs, mostly focusing on heavily obscured ones (Eguchi et al. 2009; Winter et al. 2009; Eguchi et al. 2011). A remarkable finding is the dis-

covery of “new type” AGNs that exhibit a very small amount of scattering gas, which are interpreted to have geometrically very thick tori, unlike classical type AGNs (Ueda et al. 2007; Eguchi et al. 2009).

Radio galaxies, a class of AGNs exhibiting powerful jets, are key objects to understand the origin and effects of the AGN feedback to the surroundings. However, the fundamental question, how the structure of the nucleus is different between AGNs with jets and without jets, is not fully resolved yet. This paper is the fourth in a series related to *Suzaku* and *Swift*/BAT observations of AGN, targeting two narrow line radio galaxies (type-2 radio loud AGNs) 3C 403 and IC 5063, for which no “simultaneous” broad band spectra over the 0.1–200 keV band have been reported. All targets studied in our previous series of papers are Seyfert galaxies (i.e., AGNs without powerful jets) except for NGC 612 reported in Eguchi et al. (2011). By adding these new targets, we increase the sample for comparing the statistical properties of radio loud AGNs to radio quiet ones.

3C 403 ($z = 0.059$) is a NLRG classified as “X-shaped” or “winged” radio morphology (Leahy & Williams 1984), which is explained as the results of propagation of jets in non-axisymmetric atmospheres (Kraft et al. 2005). The host galaxy Hubble type is S0 or peculiar. Vasudevan et al. (2010) obtained the mass of the SMBH to be $10^{8.26} M_\odot$ using the correlation between black hole mass and bulge luminosity, according to the procedure described in (Vasudevan & Fabian 2009). The bulge luminosity is derived from the total K-band flux in the 2MASS point source catalog by subtracting the AGN contribution estimated from the X-ray luminosity. Kraft et al. (2005) studied the X-ray properties of 3C 403 with *Chandra*, detecting X-ray emission from the nucleus, hot interstellar medium (ISM), extended radio structures (lobes and wings), and compact regions in the jet (knots and hot spots). IC 5063 ($z = 0.0110$) has a highly anisotropic ionizing radiation field with “X” or “conical” morphology (Colina et al. 1991), associated with a giant elliptical or S0 host galaxy. The black hole

¹ Department of Astronomy, Kyoto University, Kyoto 606-8502, Japan

² Department of Physics, Ehime University, Matsuyama 790-8577, Japan

³ Department of Astronomy, University of Maryland, College Park, MD, USA

TABLE 1
LIST OF TARGETS

Target Name (<i>Swift</i> ID)	3C 403 (J1952.4+0237)	IC 5063 (J2052.0-5704)
R.A. (J2000) ^a	19 52 15.809	20 52 02.34
Decl. (J2000) ^a	+02 30 24.18	-57 04 07.6
Redshift ^a	0.059	0.011348
<i>Suzaku</i> Observation ID	704011010	704010010
Start Time (UT)	2009-04-08T19:53:00	2009-04-24T15:04:25
End Time (UT)	2009-04-10T02:35:24	2009-04-25T16:28:19
Exposure ^b (XIS) (ks)	47.9	45.2
Exposure (HXD/PIN) (ks)	39.3	57.6

^a The position and redshift for each source are taken from the NASA/IPAC Extragalactic Database.

^b Based on the good time interval of XIS-0.

mass is estimated to be $10^{7.41} M_{\odot}$ (Vasudevan et al. 2010). Koyama et al. (1992) observed this object with the *Ginga* satellite and found that the energy spectrum in the 3–18 keV band is described by a power-law with a photon index of 1.5 and an absorption column density of $2 \times 10^{23} \text{ cm}^{-2}$. Vignali et al. (1997) report the results of observations with *ASCA* and *ROSAT*. From the 0.1–10 keV spectrum of IC 5063, they detect two power-law components (with photon indices of 1.7 ± 0.2 and 2.2 ± 0.3 , where the former is absorbed with $N_{\text{H}} \sim 2 \times 10^{23} \text{ cm}^{-2}$), and a narrow iron-K α line at $E_{\text{K}\alpha} \approx 6.4 \text{ keV}$ (with an equivalent width of $\sim 200 \text{ eV}$).

The organization of this paper is as follows. Section 2 summarizes the observations. Data analysis and results are presented in Section 3. We discuss the implication of our results in Section 4. The cosmological parameters (H_0 , Ω_{m} , Ω_{Λ}) = (70 km s $^{-1}$ Mpc $^{-1}$, 0.3, 0.7; Komatsu et al. 2009) are adopted in calculating the luminosities. The errors attached to spectral parameters correspond to those at 90% confidence limits for a single parameter.

2. OBSERVATIONS

Suzaku, the fifth Japanese X-ray satellite (Mitsuda et al. 2007), carries a set of X-ray CCD cameras called the X-ray Imaging Spectrometer (XIS) and a non-imaging instrument called the Hard X-ray Detector (HXD) composed of Si PIN photodiodes and Gadolinium Silicon Oxide (GSO) scintillation counters. In this paper, we analyze the data of three XISs and HXD/PIN, which cover the energy band of 0.2–10 keV and 10–60 keV, respectively. The data of HXD/GSO covering energies above 50 keV are not utilized because the fluxes of our targets are too faint to be detected. In the spectral analysis, we also use the spectra of *Swift*/BAT in the 14–195 keV band averaged for 58-months (Baumgartner et al. 2011).

The two NLRGs 3C 403 and IC 5063, cataloged in the *Swift*/BAT 9-months survey (Tueller et al. 2008), were observed with *Suzaku* in 2009 April. The basic information of our targets and observation log are summarized in Table 1. Each object was observed at the “HXD nominal” pointing position for a net exposure of $\sim 50 \text{ ks}$ after data screening.

3. ANALYSIS AND RESULTS

The data reduction was performed according to standard procedures from the cleaned event files provided by the *Suzaku* team (processing version 2.3.12.25). We used FTOOLS (heasoft version 6.8) for extraction of light

curves and spectra, and XSPEC (version 12.5.1n) for spectral fitting. The XIS events of the source were extracted from circular regions centered on the source peak with a radius of 2' (3C 403) and 2'.5 (IC 5063), in which 85% and 91% of the total source photons are accumulated by the X-ray telescopes, respectively. The background data were taken from annulus regions centered at the averaged optical axis of the X-ray telescopes with radii between 2.8'–6.7' for 3C 403 and 1.2'–6.3' for IC 5063, by excluding regions where the target and other bright sources are located. We generated the RMF files of the XIS with *xisrmfgen*, and the ARF files with *xissimarfgen* (Ishisaki et al. 2007). The “tuned” NXB event files provided by the HXD team were utilized to produce the background spectra, to which that of the cosmic X-ray background (CXB) was added based on the formula of Gruber et al. (1999). The source flux of HXD/PIN in the 15–40 keV band corresponds to $\simeq 6\%$ (3C 403) and $\simeq 24\%$ (IC 5063) of the background (NXB+CXB) rate. The signal-to-noise ratio calculated as the source photon counts divided by the square root of the total (source plus background) counts in this band is 5.3 for 3C 403 and 26.7 for IC 5063. The statistical error is larger than the systematic uncertainty of $\simeq 0.34\%$ (1σ) in the background model for a 40 ks exposure (Fukazawa et al. 2009). We used `ae_hxd_pinhxnome5_20080716.rsp` for the HXD/PIN response.

3.1. Light Curves

Figure 1 shows the light curves of 3C 403 and IC 5063 in the 2–10 keV band combined from XIS-0 and XIS-3 (upper), those in the 15–40 keV band from HXD/PIN (middle), and their hardness ratio between the two bands. A bin width of 5760 s, the orbital period of *Suzaku* (including periods of data gap that are excluded to calculate the count rate), is chosen to eliminate any systematics caused by the orbital change of the satellite. There is no evident time variability in the light curves of 3C 403, while the 2–10 keV flux of IC 5063 increases after $\sim 6 \times 10^4 \text{ s}$ from the beginning of the observation. The constant flux model is rejected by with reduced χ^2 of 6.34 with 15 degrees of freedom. Due to the limited statistics in the PIN data, however, the 15–40 keV light curve and hardness ratio of IC 5063 show no significant variability based on χ^2 tests. We examine the spectral variability of IC 5063 in Section 3.3.2.

3.2. BAT Spectra

Before performing spectral fitting to the *Suzaku* data, we analyze the *Swift*/BAT spectra in the 14–195 keV

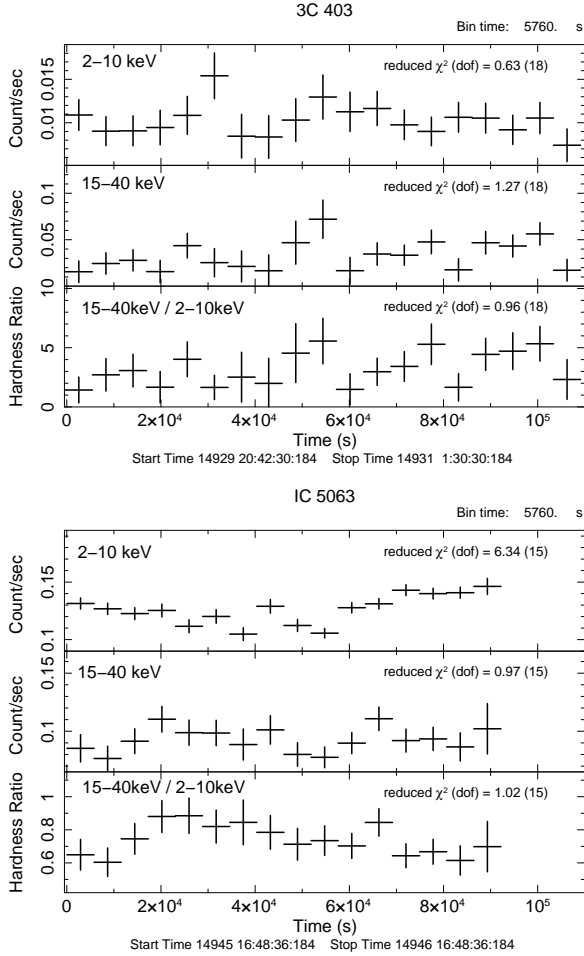


FIG. 1.— (top) Light curves of 3C 403 obtained with the XIS in the 2–10 keV band (upper) and with the HXD/PIN in the 15–40 keV band (middle), and the hardness ratio between the two bands (lower). The bin size is 5760 s. The reduced χ^2 with the degrees of freedom for the constant flux hypothesis is shown at the upper right corner in each panel. (bottom) The same as IC 5063.

band to constrain the high energy cutoff. The detection significance of 3C 403 and IC 5063 in the 58-months data is 9.6 and 26.8, respectively (Baumgartner et al. 2011). A simple power law fit with $\propto E^{-\Gamma}$ is statistically acceptable, yielding a photon index of $\Gamma = 1.7 \pm 0.3$ with $\chi^2/\text{dof} = 8.5/6$ for 3C 403, and $\Gamma = 1.9 \pm 0.1$ with $\chi^2/\text{dof} = 3.7/6$ for IC 5063. It is known, however, that the hard X-ray continuum of AGNs is generally described by a power law with an exponential cutoff, $\propto E^{-\Gamma} \exp(-E/E_{\text{cut}})$, where E_{cut} is a cutoff energy. Since the cutoff energy is typically > 100 keV (e.g., Deluit & Courvoisier 2003), the *Suzaku* data alone (XIS and HXD/PIN) cannot determine it. To fit the BAT spectra, we adopt **pexrav** model (Magdziarz & Zdziarski 1995) in XSPEC, which contains a Compton reflection component from optically thick cold matter. The strength of reflection is represented with $R \equiv \Omega/2\pi$, where Ω is the solid angle of the reflector viewed from the irradiating source. In this analysis, we assume two extreme cases for the reflection strength, $R = 0$ and 2. The inclination angle in the **pexrav** model is fixed at 60° as a representative value throughout our

TABLE 2
CUTOFF ENERGIES (E_{cut}) ESTIMATED BY THE BAT SPECTRA

	Target Name	3C 403	IC 5063
$R = 0$	E_{cut}	540(> 120)	220^{+250}_{-80}
	χ^2/dof	8.9/6	3.3/6
$R = 2$	E_{cut}	570(> 140)	190^{+140}_{-60}
	χ^2/dof	8.6/6	12.9/6

NOTE. — The photon index is fixed at 1.7 for both targets.

paper except in Section 3.4. To avoid strong coupling between E_{cut} and Γ , we adopt $\Gamma = 1.7$ for both targets, which is an averaged value of 13 nearby radio galaxies obtained from previous X-ray studies (Grandi et al. 2006). As summarized in Table 2, we find that $E_{\text{cut}} > 120$ keV for 3C 403 and $E_{\text{cut}} = 130\text{--}470$ keV for IC 5063. In the following spectral analysis, we fix the cutoff energy at 200 keV for both 3C 403 and IC 5063, since changing these values within the above uncertainties does not affect our conclusions.

3.3. Spectral Analysis with Analytic Models

For spectral analysis, we use the *Suzaku* spectra of the 2 XIS-FIs in the 1–11 keV band, and the XIS-BI in the 0.5–8 keV band, and HXD/PIN in the 16–40 keV band, where the highest signal-to-noise ratios are achieved. The XIS data in the 1.7–1.9 keV band are discarded because of calibration uncertainties associated with the instrumental Si-K edge. The relative flux normalization of the XIS-BI to the XIS-FIs is set free, while that of the HXD/PIN to the XIS-FIs is fixed at 1.18 based on the calibration using the Crab Nebula (Maeda et al. 2008). The Galactic absorption, $N_{\text{H}}^{\text{Gal}}$, is included in the spectral model, which is fixed at the value derived from the H I map of Kalberla et al. (2005) ($N_{\text{H}}^{\text{Gal}} = 1.22 \times 10^{21}$ cm $^{-2}$ for 3C 403 and 6.10×10^{20} cm $^{-2}$ for IC 5063). Solar abundances by Anders & Grevesse (1989) are assumed throughout our analysis. The upper panels of Figure 2 plot the *Suzaku* spectra of the two sources folded with the detector responses, together with the BAT spectra in units of photons cm $^{-2}$ s $^{-1}$.

We apply the three analytic models defined in Eguchi et al. (2009), Models A, B, and C (see below), to which we add a spectral component from an optically thin plasma with Solar abundances (**apec**) because it improves the fit significantly in both targets. In the case of 3C 403, two power law components from the radio lobes/wings and from the compact structures in the jets are also included. These $\sim 10''$ scale structures are spatially resolved in the *Chandra* data (Kraft et al. 2005); their fluxes in the 0.25–10 keV band are estimated to be $(4.4 \pm 0.3) \times 10^{-14}$ erg cm $^{-2}$ s $^{-1}$ and $(3.5 \pm 0.3) \times 10^{-14}$ erg cm $^{-2}$ s $^{-1}$, corresponding to 0.31% and 0.27% of the total flux from the unresolved nucleus corrected for absorption, respectively.

Model A consists of a direct component from the nucleus (a cutoff power law absorbed by cold matter), a scattered component (a cutoff power law without absorption), and an iron-K emission line (a Gaussian). The high energy cutoff is fixed at 200 keV based on the BAT only results (see above). The scattered component is assumed to have the same slope as the direct one with

a fraction of f_{scat} . In Model B, a Compton reflection component of the direct continuum from optically thick matter (**pexrav** model), absorbed with a column density of $N_{\text{H}}^{\text{refl}}$, is further added to Model A. This emission is expected from the inner wall of the torus and/or the accretion disk irradiated by the central source. The absorption for the reflection component is set to be independent of that of the transmitted one, because the emission region is different and the line-of-sight column density may not always be the same, depending on the viewing geometry. Model C has the same emission components as Model B including an absorbed reflection component, but we consider two layers of absorber with different hydrogen column densities for the transmitted component, corresponding to the “partial covering” case where the absorbers in the line of sight consist of gas blobs smaller than the size of the X-ray emitting region (e.g., Elitzur & Shlosman 2006).

We first perform simultaneous fit only to the *Suzaku* XIS and HXD/PIN spectra to select the most appropriate model for each object among the three. To avoid complex effects of time variability, the BAT spectra averaged for 58 months are not utilized in this stage. We start from the simplest model (Model A), and adopt a more complex model (Models B or C) only if we find a statistically significant improvement of the fit or a physically more reasonable solution. After selecting the best model describing the data in this way, we finally include the BAT spectra in the joint fit to better constrain the continuum up to 200 keV. We allow only the normalization of the direct component to vary while keeping the continuum shape (i.e., spectral slope and cutoff energy) the same between the *Suzaku* and *Swift*/BAT epoch. The normalizations of the reflection and scattered component are also linked between *Suzaku* and *Swift*/BAT, considering that the time scale of their variability should be larger than $>$ years if the emission region size is typical (>1 pc) of the scale size of tori. Unlike our previous papers (Ueda et al. 2007; Eguchi et al. 2009, 2011), we define the reflection strength and scattered fraction relative to the BAT flux, not to the *Suzaku* flux, since the BAT spectra integrated over 58 months should be a good indicator of the averaged flux level responsible for these reprocessed emission.

3.3.1. 3C 403

From the results by Kraft et al. (2005) obtained with *Chandra*, we are able to estimate the X-ray fluxes from the radio lobes/wings and compact features in the jets (knots and hot spots) that should contribute to the *Suzaku* spectra, where these jet-related structures and the nucleus are not spatially resolved. Since neither of these components are expected to be variable on time scale of years, we fix their fluxes at the best-fit *Chandra* values; we confirm that the uncertainties do not affect our results as their contributions in the total flux are minor. The component from the radio lobes/wings and jets are represented as a power law with a photon index of 1.8 and 2.0 with a normalization at 1 keV of 9.8×10^{-15} and $9.6 \times 10^{-15} \text{ erg cm}^{-2} \text{ s}^{-1} \text{ keV}^{-1}$, respectively, both are always added to the above three models representing the nucleus emission. Since photon index of the power law in the lobes/wings component is poorly constrained from the *Chandra* data, we fix its

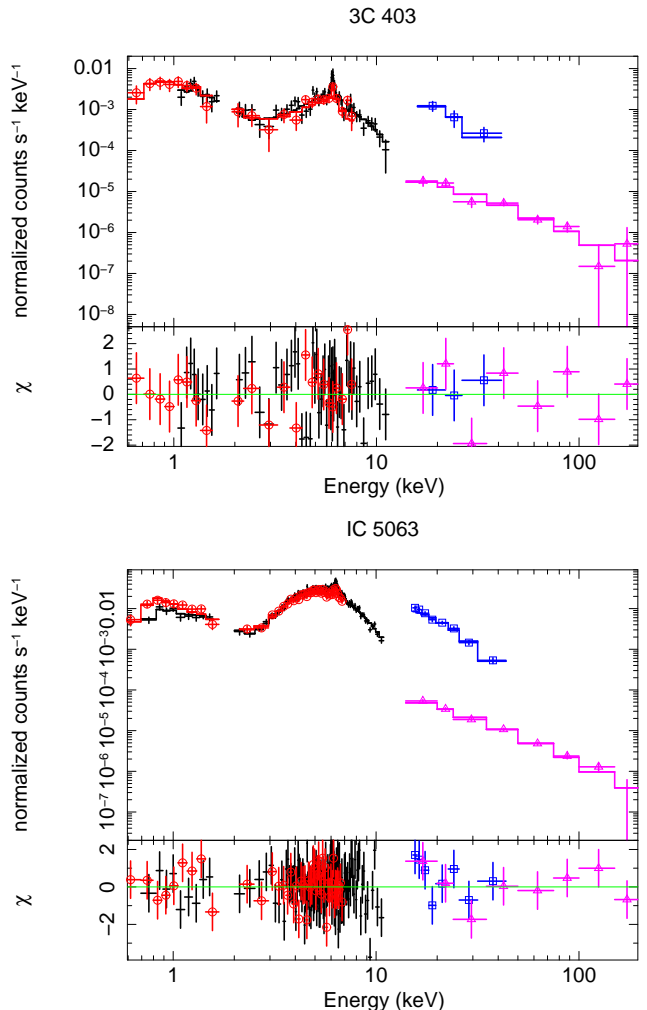


FIG. 2.— (top) The folded spectra of 3C 403 obtained with the XIS-FIs in the 1–11 keV band (black), the XIS-BI in the 0.5–8 keV band (red, open circles), the HXD/PIN in the 16–40 keV band (blue, open squares), and the *Swift*/BAT in the 14–195 keV band (magenta, open triangles). The best-fit model (B in Table 3) is plotted by the solid lines, and the residuals in units of χ are shown in the lower panels. (bottom) The same as IC 5063.

slope to that of the radio emission Dennett-Thorpe et al. (2002), assuming that the radio and X-ray emission correspond to the synchrotron and inverse Comptonization from the same electrons, respectively. To model optically thin thermal emission from the hot interstellar medium (ISM) detected by Kraft et al. (2005), we also add an **apec** model whose temperature and emission measure are free parameters. The elemental abundances are fixed at the Solar values.

We adopt Model B as the most appropriate model for the nucleus emission of 3C 403. Model A yields a very small photon index of the transmitted component, ~ 1.0 , which seems rather unphysical, with $\chi^2/\text{dof} = 82/73$. Reasonable results are obtained with Model B, which gives a photon index of ~ 1.5 with $\chi^2/\text{dof} = 74/71$. Model C does not improve the fit significantly in terms of the χ^2 value ($\chi^2/\text{dof} = 74/69$). The best fit model (Model B + two power laws + **apec**) to the joint fit including the *Swift*/BAT spectrum is overplotted in the up-

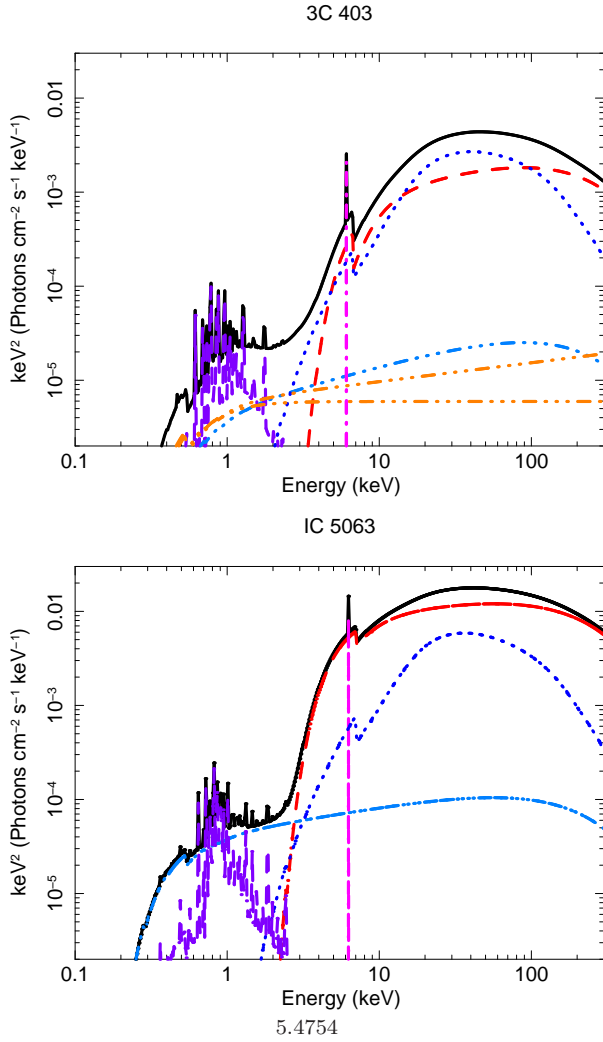


FIG. 3.— (top) Best-fit analytic model for 3C 403 in units of $EF(E)$ ($F(E)$ is the energy flux at the energy E). The solid (black), dashed (red), dotted (blue), and dot-dashed (magenta) curves correspond to the total, direct component, reflection component, and iron-K emission line. The dashed (purple) curve represents the emission from an optically thin thermal plasma, and dot-dot-dot-dashed (orange) curves show the emission from the jets and radio lobes/wings (see the text). The dot-dot-dot-dashed (cyan) curve represents the scattered component. (bottom) The same as IC 5063.

per panel of Figure 2 with residuals in the lower panel. Figure 3 (a) plots its $EF(E)$ form, where $F(E)$ is the energy flux at the energy E .

The best-fit parameters are summarized in Table 3. The moderately flat photon index ($\Gamma = 1.53^{+0.03}_{-0.02}$), though within the typical range for radio galaxies (Grandi et al. 2006), may be affected by simplification of the analytic model where only a single absorber is assumed for the reflection component. The scattered fraction $f_{\text{scat}} \sim 0.4\%$ is rather small, corresponding to that of a “new type” AGN in Ueda et al. (2007) if it corresponds to the opening angle of the torus. This issue will be discussed in Section 4. The iron-K emission line is detected at ≈ 6.4 keV and is narrow (with a 1σ width of <98 eV at 90% confidence level). This indicates that it mainly comes from cold and distant matter from

the black hole, fully consistent with a torus origin. The equivalent width of the iron-K line with respect to the reflection continuum is 1.13 ± 0.24 keV, which is physically self-consistent according to theoretical calculations (e.g., Ikeda et al. 2009). The smaller column density for the reflected component ($N_{\text{H}}^{\text{refl}} \sim 4 \times 10^{22} \text{ cm}^{-2}$) than that for the transmitted one ($N_{\text{H}} \approx 6 \times 10^{23} \text{ cm}^{-2}$) suggests that we are looking at the source with a somewhat face-on geometry so that a significant fraction of the reflected light from the inner wall of the torus can reach us without strong obscuration.

While we detect a very strong reflection within the *Suzaku* spectra corresponding to $R \approx 2$, which dominates the HXD/PIN flux, we find a lower value of $R \approx 0.6$ when normalized to the flux of the transmitted component determined by *Swift*/BAT. This can be explained by time variability since the flux during the *Suzaku* observation was about 3 times smaller than the averaged flux over the 58 months of the BAT observations. In fact, the difference between the unabsorbed nuclear flux in the 0.25–10 keV band was $1.3 \times 10^{-11} \text{ erg cm}^{-2} \text{ s}^{-1}$ at the *Chandra* observation in 2002, while that measured with *Suzaku* is $4.0 \times 10^{-12} \text{ erg cm}^{-2} \text{ s}^{-1}$.

The best fit temperature of the **apec** component is $kT = 0.29 \pm 0.03$ keV, consistent with the *Chandra* result (Kraft et al. 2005), $kT = 0.3 \pm 0.04$ keV. We note, however, that its flux as determined with *Suzaku*, $2.8 \times 10^{-13} \text{ erg cm}^{-2} \text{ s}^{-1}$ in the 0.25–10 keV band, is about 5 times higher than that estimated from the *Chandra* data, even taking into account the contribution from the hot ISM in an outer region at radii larger than $7''.5$ up to $60''$ from the nucleus (see Kraft et al. (2005) Section 3.1), which is contained in the *Suzaku* extraction region. We find that this discrepancy is mainly produced due to the spectral coupling with the unabsorbed soft component; its slope is assumed to be the same as for the direct component in our spectral model, $\Gamma = 1.5$, which is smaller than that adopted by Kraft et al. (2005), $\Gamma = 2.0$. Thus, the difference may be regarded as a systematic uncertainty in the absolute flux from the hot ISM, whose core emission is difficult to spatially resolve even with *Chandra* from the AGN component. We confirm that our result on the amount of the scattering gas presented in Section 3.3.1 is not significantly affected (within a factor of 1.5) even when we fix the flux of the **apec** component at the *Chandra* value in the spectral analysis.

3.3.2. IC 5063

Model B with thin thermal emission (**apec**) is adopted as the best model for IC 5063 from the time averaged *Suzaku* spectra. The thermal emission is required because it significantly reduces χ^2 in all 3 models (A, B, and C) and its addition produces acceptable fits. Models A, B, and C give $\chi^2/\text{dof} = 185.8/177$, $175/175$ and $175/173$, respectively. Thus, the improvement of the fit by adding a reflection component (Model B) is found to be significant with an F-test probability of 0.007, whereas the introduction of an additional absorber for the transmitted component (Model C) is not significant in introducing χ^2 . The results of simultaneous analysis of the *Suzaku* and BAT spectra with Model B + **apec** are summarized in Table 3, and the best-fit model is plotted in Figures 2 and 3.

TABLE 3
BEST-FIT PARAMETERS OF *Suzaku* AND *Swift*/BAT SPECTRA WITH ANALYTIC MODEL

	Target	3C 403	IC 5063
	Best-fit model	B + apec + two power laws	B + apec
(1)	$N_{\text{H}}^{\text{Gal}} (10^{22} \text{ cm}^{-2})$	0.122	0.061
(2)	$N_{\text{H}} (10^{22} \text{ cm}^{-2})$	61^{+6}_{-5}	25.0 ± 0.7
(3)	Norm _{BAT}	3.2 ± 0.7	1.06 ± 0.08
(4)	Γ	$1.53^{+0.03}_{-0.02}$	1.72 ± 0.02
(5)	$f_{\text{scat}} (\%)$	0.4 ± 0.3	0.9 ± 0.1
(6)	$E_{\text{cen}} (\text{keV})$	$6.43^{+0.04}_{-0.02}$	$6.39^{+0.02}_{-0.08}$
(7)	$E_{\text{wid}} (\text{eV})$	< 98	< 78
(8)	EW (eV)	455 ± 98	148 ± 20
(9)	EW ^{refl} (keV)	1.13 ± 0.24	1.52 ± 0.21
(10)	$N_{\text{H}}^{\text{refl}} (10^{22} \text{ cm}^{-2})$	$3.6^{+4.2}_{-2.8}$	$3.1^{+3.4}_{-1.9}$
(11)	R	0.65 ± 0.17	0.65 ± 0.13
(12)	$kT (\text{keV})$	0.29 ± 0.03	$0.61^{+0.07}_{-0.08}$
(13)	$n^2V (\text{cm}^{-3})$	$(2.7 \pm 0.7) \times 10^{65}$	$(1.0 \pm 0.2) \times 10^{63}$
(14)	$F_{2-10} (\text{erg cm}^{-2} \text{ s}^{-1})$	7.14×10^{-13}	8.03×10^{-12}
(15)	$F_{10-50} (\text{erg cm}^{-2} \text{ s}^{-1})$	7.96×10^{-12}	3.76×10^{-11}
(16)	$L_{2-10} (\text{erg s}^{-1})$	1.76×10^{43}	5.61×10^{42}
	χ^2/dof	81.7/78	182.6/182

NOTE. — Errors correspond to 90% confidence level for a single parameter. Both f_{scat} and R are normalized to the direct component flux as measured with BAT.

- (1) The hydrogen column density of Galactic absorption by Kalberla et al. (2005).
- (2) The line-of-sight hydrogen column density for the direct component.
- (3) Normalization ratio of the direct component between the BAT and *Suzaku* spectra.
- (4) The power-law photon index of the direct component.
- (5) The fraction of the scattered component relative to the intrinsic power law.
- (6) The center energy of the iron-K α emission line at the rest frame.
- (7) The observed width of iron-K α line. This is fixed at 1 eV when we determine the continuum parameters.
- (8) The observed equivalent width of the iron-K α line.
- (9) The observed equivalent width of the iron-K α line with respect to the reflection component.
- (10) The line-of-sight hydrogen column density for the reflection component.
- (11) The relative strength of the reflection component to the direct one, defined as $R \equiv \Omega/2\pi$, where Ω is the solid angle of the reflector.
- (12) The temperature of the **apec** component.
- (13) The emission measure of the **apec** component.
- (14) The observed *Suzaku* flux in the 2–10 keV band.
- (15) The observed *Suzaku* flux in the 10–50 keV band.
- (16) The 2–10 keV intrinsic luminosity obtained with *Suzaku*, corrected for the absorption.

The best fit photon index of $\Gamma \approx 1.7$ from IC 5063 is typical of radio galaxies. The scattered fraction $f_{\text{scat}} \sim 0.9\%$ is larger than that of 3C 403. It is consistent with the *ASCA* result of $\sim 1\%$ (Vignali et al. 1997). The narrow iron-K line detected at 6.4 keV is consistent with being emitted from the torus. Its equivalent width with respect to the reflected continuum (1.5 ± 0.2 keV) is within a range of theoretical expectation, thus supporting the validity of our spectral model. Similar to the case of 3C 403, the reflection component is less absorbed ($N_{\text{H}}^{\text{refl}} \approx 3 \times 10^{22} \text{ cm}^{-2}$) compared with the transmitted component ($N_{\text{H}} \approx 3 \times 10^{23} \text{ cm}^{-2}$), and disfavoring the likely edge-on geometry. The reflection strength of $R \approx 0.6$ relative to the averaged BAT flux is close to the value obtained from 3C 403. These results suggest that the torus geometry of the two AGNs could be similar to each other. The obtained temperature and luminosity of the **apec** component are in the typical range of hot ISM detected from elliptical galaxies (Matsushita et al. 2000) and hence supports this interpretation of its origin, although we cannot rule out the possibility that a part of this emission may come from photoionized plasma irradiated by the AGN, which should be regarded as an accompanying component of the scattered emission. Nevertheless, since the amplitude of the scattered fraction is mainly determined from the spectrum in 1–2 keV band,

where no strong emission lines are present, its intensity is not strongly affected by the uncertainty in the nature of the line emitting component.

Since IC 5063 exhibits significant time variability during the *Suzaku* observation, we check time variability of the spectra by dividing the time region into two states with different flux levels, epoch I (for 57.6 ks from the beginning) and epoch II (after that). We adopt the Model B + **apec** model for each spectrum. Assuming that the reflection component and thin thermal emission were not variable on this short time scale, since they most probably originate from the torus and host galaxy, respectively, we fix the spectral parameters of these components (and its absorption) at the best-fit values determined by the time-averaged *Suzaku* (and *Swift*/BAT) spectra. We find that the shape of the transmitted component did not show variability within statistical errors, $\Gamma = 1.7 \pm 0.1$ and $N_{\text{H}} = (26 \pm 2) \times 10^{22} \text{ cm}^{-2}$ in epoch I and $\Gamma = 1.8 \pm 0.1$ and $N_{\text{H}} = (25 \pm 2) \times 10^{22} \text{ cm}^{-2}$ in epoch II, and only the normalization changed between the two epochs. Thus, averaging the *Suzaku* spectra over the whole epoch is justified.

3.4. Application of Torus Model

We also fit the spectra generated by the Monte-Carlo model of Ikeda et al. (2009), where reflection compo-

TABLE 4
BEST-FIT PARAMETERS OF *Suzaku* AND *Swift*/BAT SPECTRA WITH TORUS MODEL

		3C 403	IC 5063
(1)	Model	Solar + apec ^a + two power laws	Solar + apec ^a
(2)	$N_{\text{H}}^{\text{Gal}} (10^{22} \text{ cm}^{-2})$	0.122 ^b	0.061 ^b
(3)	$N_{\text{H}}^{\text{eq}} (10^{22} \text{ cm}^{-2})$	67 ± 25	25^{+10}_{-1}
(4)	θ_{oa} (degrees)	50 ^b	50 ^b
(5)	θ_{inc} (degrees)	51^{+17}_{-0}	65^{+18}_{-14}
(6)	Norm _{BAT}	3.2 ± 1.2	$1.04^{+0.16}_{-0.15}$
(7)	Γ	$1.55^{+0.32}_{-0.05}$	$1.82^{+0.15}_{-0.11}$
(8)	$f_{\text{scat},0} (\%)$	$0.3 (< 0.7)$	0.5 ± 0.1
(9)	E_{cen} (keV)	6.4 ^b	6.4 ^b
(10)	ϵ_{Fe}	$1.2^{+0.7}_{-0.5}$	$1.2^{+0.2}_{-0.3}$
	χ^2/dof	88.4/80	182.0/187

NOTE. — Errors are 90% confidence level for a single parameter. $f_{\text{scat},0}$ is normalized to the direct component flux as measured with BAT.

(1) The model used in the fit. “Solar” means the torus model with Solar abundances.

(2) The hydrogen column density of Galactic absorption by Kalberla et al. (2005).

(3) The hydrogen column density of the torus along the equatorial direction.

(4) The half opening angle of the torus.

(5) The inclination angle of the torus. The lower limit is restricted to be 51° by the condition $\theta_{\text{inc}} > \theta_{\text{oa}} + 1$.

(6) Normalization ratio of the direct component between the BAT and *Suzaku* spectra.

(7) The power-law photon index. It is restricted in the range of 1.5–2.5 in the table model.

(8) The fraction of the scattered component relative to the intrinsic power law when the half opening angle of the torus is 45° .

(9) The center energy of the iron-K emission line at the rest frame of the source redshift.

(10) The relative strength of the iron-K emission line to that predicted by the torus model.

^a The parameters of the **apec** model are fixed at those in Table 3.

^b The parameters are fixed at this value.

nents from a three-dimensional, axially symmetric torus around the nucleus emitting a cutoff power law continuum is computed. The torus has four parameters, the half opening angle (θ_{oa}), inclination (θ_{inc}), total column density in the equatorial plane (N_{H}^{eq}), and the ratio between the outer and inner radii, which is fixed to be 100 (for definition, see Figure 2 of Ikeda et al. (2009)).

We analyze the data in the same manner as described in Eguchi et al. (2011), to which we refer the reader for details of the spectral formula in the XSPEC terminology. The unabsorbed and absorbed reflection continua and fluorescence iron-K line from the torus are included in the model as separate components. The line-of-sight column density of the direct component is automatically determined from the four geometrical parameters of the torus; for absorbed AGNs $\theta_{\text{oa}} < \theta_{\text{inc}}$. The observed scattered component is represented as $f_{\text{scat}} = f_{\text{scat},0}(1 - \cos \theta_{\text{oa}})/(1 - \cos 45^\circ)$, where $f_{\text{scat},0}$ reflects the averaged column density of the scattering gas. The reflection component from the accretion disk is also considered for the direct component by assuming a solid angle of $\Omega = 2\pi$ with the same inclination as for the torus. Solar abundances are assumed. We fit the *Suzaku* (XIS and HXD/PIN) and *Swift*/BAT spectra simultaneously by limiting the energy band to 0.5–100 keV to which the Ikeda model is applicable. Although the model uses a cutoff energy of 360 keV instead of 200 keV, the effect is negligible as we only use energies below 100 keV. Similar to the analysis in Section 3.3, time variability of the flux of the direct component between the *Suzaku* and *Swift*/BAT epochs is taken into account with an assumption that the power law slope is constant. The **apec** component and the two power law components originating from the radio lobes/wings and resolved jet components (for 3C 403) are included in the spectral model, whose parameters are fixed at the values found in Section 3.3.1.

We find that this “torus model” also provides a good fit to the observed spectra of 3C 403 and IC 5063 with $\chi^2/\text{dof}=88/80$ and $182/187$, respectively. The torus opening angle is not well determined in the model due to the limited photon statistics and we fixed it at $\theta_{\text{oa}} = 50^\circ$ in our analysis consistent with the optical observations of the ionized cone in IC 5063 ($\sim 50^\circ$; Colina et al. 1991). The free parameters of the spectral model are θ_{inc} , N_{H}^{eq} , $f_{\text{scat},0}$, the normalization ratio between the iron-K emission line and reflected continuum (ϵ_{Fe}), the photon index (Γ), and two normalizations of the cutoff power law for the *Suzaku* and *Swift*/BAT data. The best-fit parameters are summarized in Table 4. We find $f_{\text{scat},0} = 0.3 (< 0.7)\%$ ($1.0^{+0.8\%}_{-0.5\%}$) for 3C 403 and $f_{\text{scat},0} = 0.5 \pm 0.1\%$ ($0.6^{+0.1\%}_{-0.2\%}$) for IC 5063 when normalized to the BAT (or *Suzaku*) flux. These results on the scattering gas will be discussed in Section 4. In both targets, the best-fit photon index becomes slightly larger than in the analytical model, although the difference is within the statistical errors. The normalization ratio of the direct component between the BAT and *Suzaku* spectra is consistent with that obtained from the analytic model. As discussed in the previous subsections, the data indeed favor an inclination angle that is only slightly larger than the torus opening angle, particularly for 3C 403.

A similar numerical torus model by Murphy & Yaqoob (2009) (MYTORUS in XSPEC) also gives a good fit for both targets, where a slightly different torus geometry is assumed with a fixed opening angle of 60° . By adopting it instead of the Ikeda model in the same way, we obtain $\Gamma = 1.7^{+0.1}_{-0.3}$, $\theta_{\text{inc}} = 75^{+10}_{-14}$ deg, and $N_{\text{H}}^{\text{eq}} = 0.8^{+2.1}_{-0.3} \times 10^{24} \text{ cm}^{-2}$ for 3C 403 with $\chi^2/\text{dof}=85.5/79$, and $\Gamma = 1.9 \pm 0.1$, $\theta_{\text{inc}} = 63^{+9}_{-2}$ deg, and $N_{\text{H}}^{\text{eq}} = 0.6^{+0.6}_{-0.2} \times 10^{24} \text{ cm}^{-2}$ for IC 5063 with $\chi^2/\text{dof}=182.3/183$. These parameters are consistent with those obtained by the Ikeda model within

the statistical errors, except for N_{H}^{eq} of IC 5063.

4. SUMMARY AND DISCUSSION

With *Suzaku*, we have for the first time obtained simultaneous broad band X-ray spectra from two NLRGs, 3C 403 and IC 5063, with CCD energy resolution below 10 keV. Combined with the *Swift*/BAT spectra averaged for 58 months, we are able to best constrain the spectral properties over the 0.5–200 keV band. The bolometric luminosities of 3C 403 and IC 5063 are estimated as $10^{45.1}$ erg s $^{-1}$ and $10^{44.3}$ erg s $^{-1}$ from the infrared and X-ray luminosities (Vasudevan et al. 2010), corresponding to the Eddington fractions of approximately 0.06, using the black hole masses estimated by Vasudevan et al. (2010). These Eddington fractions are in the range observed for radio galaxies (e.g., Evans et al. 2006) and for Seyfert galaxies (Winter et al. 2009) in the local universe. Our targets thus significantly increase the NLRG sample with similar Eddington fractions studied with *Suzaku* and *Swift*/BAT in addition to NGC 612, which has $L_{\text{bol}}/L_{\text{Edd}} = 0.02$ and $L_{\text{bol}} = 10^{44.5}$ erg s $^{-1}$ (Vasudevan et al. 2010).

While *Suzaku* provide us with unique spectroscopic data, the integrated spectra from radio galaxies inevitably contain the contribution from various components besides the nucleus, such as the hot ISM, the radio lobes/wings, and the kpc-scale jets, due to the limited spatial resolution. The thermal emission is important only in the softest energy band in the *Suzaku* data. In the case of 3C 403, we are able to separate those from the radio lobes/wings and kpc-jets, utilizing the *Chandra* results (Kraft et al. 2005). We find that the relative fluxes of these components are 1.0% and 0.7% of the unabsorbed nucleus emission at 5 keV, respectively, and thus make only minor contribution in the hard X-ray spectra. Although we cannot do the same analysis for IC 5063 and NGC 612 due to the lack of *Chandra* data, we estimate that the inverse Compton component originating from the radio lobes is 0.1% and 1% of the nucleus emission at 5 keV, respectively, using the observed radio spectra from the lobes (Jones & McAdam 1992) and a typical X-ray (inverse Compton) to radio (synchrotron) flux ratio of the lobe emission (Isobe 2002). One should note, however, that emission from the “nucleus” may also contain components from the pc-scale jets, which are seen in the VLBI images (Tarchi et al. 2007; Oosterloo et al. 2000) but cannot be resolved with *Chandra*. In fact, Evans et al. (2006) and Hardcastle et al. (2009) suggest that the unabsorbed soft X-ray components of radio galaxies is mainly attributable to the unresolved jets, based on the correlation between the soft X-ray and radio core luminosities at 5 GHz. In this context, the “scattered fraction” we discuss in our paper is only an upper limit.

For 3C 403, we can compare our results of the scattered fraction and absorption column density of the transmitted component obtained through X-ray spectroscopy with those estimated by Marchesini et al. (2005) from the near-infrared (NIR) and optical imaging data. Marchesini et al. (2005) calculate the scattered fraction and extinction from the “observed” ratios of the optical (continuum or line) luminosity to the NIR one, assuming the typical “intrinsic” luminosity ratios obtained for radio loud AGNs. Our result, $f_{\text{scat}} = (0.4 \pm 0.3)\%$, is smaller than their estimate,

$0.88^{+0.32}_{-0.23}\%$, though within the errors. This possible discrepancy may be explained if there is another unabsorbed component in the NIR/optical lights in addition to the scattered one, such as thermal emission from hot dust in the torus, and/or if there was time variability in the direct NIR/optical fluxes, which were measured from short term observations. The column density derived from the X-ray data is ~ 10 times larger than that converted from the estimated extinction, $A_V = 21.9$ mag, assuming the Galactic standard relation $A_V = 5 \times 10^{-22} N_{\text{H}}$ (Bohlin et al. 1978). This suggests much smaller dust-to-gas ratio in the torus than Galactic gas, as reported for many other AGNs (e.g., Maiolino et al. 2001).

Applying analytic spectral models that are commonly used to represent the X-ray nuclear spectra of AGNs (i.e., a cutoff power law and reflection component), we constrain the reflection strength in terms of the solid angle of the reflector to be $R \equiv \Omega/2\pi \approx 0.6$ for both 3C 403 and IC 5063. A similar value ($R \approx 0.5$ when normalized to the BAT flux) is obtained for NGC 612 by Eguchi et al. (2011), while a weaker reflection ($R < 0.4$ at 90% confidence limit) is found from another NLRG, 3C 33. These results suggest that a major fraction of NLRGs show only a moderately strong reflection component in their X-ray spectra, like many Seyfert 2 galaxies (Dadina 2007), implying that their tori have a sufficiently large solid angle to produce the reprocessed emission. Thus, there is no evidence that the torus structure is systematically different between radio galaxies and Seyfert galaxies, although studies of a larger NLRG sample are required to investigate this issue. The reason for the weak reflection in 3C 33 is unclear but may be connected to its high X-ray luminosity ($L \sim 4 \times 10^{44}$ erg s $^{-1}$ in the 2–100 keV band) compared with the other NLRGs.

The application of the numerical torus model where a realistic geometry is assumed gives useful insights into the torus structure, as demonstrated in our previous studies (e.g., Ikeda et al. 2009; Awaki et al. 2009; Eguchi et al. 2011). For our targets, we cannot constrain the torus opening angle due to the limited photon statistics; in 3C 403 since values of $\theta_{\text{oa}} = 30^\circ$, 50° , or 70° yields a very similar χ^2 value, and thus we cannot determine if the torus of 3C 403 is close to that of “new type” AGNs or to “classical type” (Ueda et al. 2007; Eguchi et al. 2009) from our data alone. As for IC 5063 we have a reasonable constraint on the torus geometry from the measurement of the ionization cone, $\theta_{\text{oa}} = 50^\circ$. Together with the fact that NGC 612 has $\theta_{\text{oa}} > 58^\circ$ (Eguchi et al. 2011), we do not find any evidence for the presence of “new type” AGNs in NLRGs studied with *Suzaku* so far, although we cannot rule out its possibility for 3C 403. We need a large sample with good quality broad band spectra to verify whether or not the distribution of population is bimodal with “new type” and “classical type” as proposed by Eguchi et al. (2009), both for radio quiet and loud AGNs.

A notable feature seen in 3C 403, IC 5063, and NGC 612, is the small amount of scattering gas, parameterized as $f_{\text{scat},0}$, reflecting the averaged column density of the scattering gas. We find $f_{\text{scat},0} < 0.7\%$ in these radio galaxies, which is systematically smaller than that obtained for Seyfert galaxies fitted with the same model, $> 2.0\%$ for NGC 3081 (Eguchi et al. 2011) and $1.3^{+0.3}_{-0.4}\%$

for *SWIFT* J0255.2–0011 (Eguchi 2011), in which the scattered component is normalized to the flux as measured with BAT. As mentioned above, one must take this value only as an upper limit considering the possible contribution from the unresolved jets to the soft X-ray component. The $f_{\text{scat},0}$ value depends on the torus opening angle assumed, but the above conclusion is unchanged unless $\theta_{\text{oa}} \ll 30^\circ$ for 3C 403. Our result suggests that there is intrinsically little “normal” gas around the nucleus in radio galaxies. This result may be explained by the jet activity which can expel such gas.

We note that the obtained reflection strengths and scattered fractions in 3C 403 and IC 5063 are normalized to the hard X-ray flux over 58 months obtained through the *Swift*/BAT monitoring, which should give a good measure of the “averaged” activity of each source. In fact, without the *Swift*/BAT data, we obtain an apparently very strong reflection strength $R \sim 2$ from 3C 403. We demonstrate that such an unphysically large R value

can indeed be accounted for by time variability, as discussed in e.g., Ueda et al. (2007); the flux of the direct component was much fainter than the average flux in the past that is responsible for the reprocessed emission from large scale ($> \text{pc}$) surroundings. Thus, the combination of the simultaneously obtained *Suzaku* spectra and the long averaged *Swift*/BAT is necessary to estimate a “true” reflection strength and scattered fraction that are free from the effects of short-term time variability.

We thank Dr. Wayne Baumgartner for sending us the *Swift*/BAT spectra of 3C 403 and IC 5063 when the web server was down. This work was partly supported by the Grant-in-Aid for Scientific Research 20540230 (YU) and 20740109 (YT), and by the grant-in-aid for the Global COE Program “The Next Generation of Physics, Spun from Universality and Emergence” from the Ministry of Education, Culture, Sports, Science and Technology (MEXT) of Japan.

REFERENCES

- Anders, E., & Grevesse, N. 1989, *Geochim. Cosmochim. Acta*, 53, 197
- Awaki, H., Terashima, Y., Higaki, Y., & Fukazawa, Y. 2009, *PASJ*, 61, 317
- Baumgartner, W., et al. 2011, *ApJS*, submitted
- Bohlin, R. C., Savage, B. D. & Drake, J. F. 1978, *ApJ*, 224, 132
- Colina, L., Sparks, W. B., & Macchetto, F. 1991, *ApJ*, 370, 102
- Dadina, M. 2007, *A&A*, 461, 1209
- Davies, R. I., Müller Sánchez, F., Genzel, R., Tacconi, L. J., Hicks, E. K. S., Friedrich, S., & Sternberg, S. 2007, *ApJ*, 671, 1388
- Dennett-Thorpe, J., Scheuer, P. A. G., Laing, R. A., Bridle, A. H., Pooley, G. G., & Reich, W. 2002, *MNRAS*, 330, 609
- Di Matteo, T., Springel, V., & Hernquist, L. 2005, *Nature*, 433, 604
- Deluit, S., & Courvoisier, T. J. L. 2003, *A&A*, 339, 77
- Eguchi, S., Ueda, Y., Terashima, Y., Mushotzky, R., & Tueller, J. 2009, *ApJ*, 696, 1657
- Eguchi, S., Ueda, Y., Awaki, H., Aird, J., Terashima, Y., & Mushotzky, R. 2011, *ApJ*, 729, 31
- Eguchi, S. 2011, Doctoral Thesis, Kyoto University
- Elitzur, M., & Shlosman, I. 2006, *ApJ*, 648, 101
- Evans, D. A., Worrall, D. M., Hardcastle, M. J., Kraft, R. P., & Birkinshaw, M. 2006, *ApJ*, 642, 96
- Fukazawa, Y., et al. 2009, *PASJ*, 61, 17
- Grandi, P., Malaguti, G., & Fiocchi, M. 2006, *ApJ*, 642, 113
- Gruber, D. E., Matteson, J. L., Peterson, L. E., & Jung, G. V. 1999, *ApJ*, 520, 124
- Hardcastle, M. J., Evans, D. A., & Croston, J. H. 2009, *MNRAS*, 396, 1929
- Ikedo, S., Awaki, H., & Terashima, Y. 2009, *ApJ*, 692, 608
- Imanishi, M., & Wada, K. 2004, *ApJ*, 617, 214
- Ishisaki, Y., et al. 2007, *PASJ*, 59, 113
- Isobe, N. 2002, Doctoral Thesis, University of Tokyo
- Jones, P. A., & McAdam, W. B. 1992, *ApJS*, 80, 137
- Kalberla, P. M. W., Burton, W. B., Hartmann, D., Arnal, E. M., Bajaja, E., Morras, R., Pöppel, W. G. L. 2005, *A&A*, 440, 775
- Komatsu, E., et al. 2009, *ApJ*, 180, 330
- Koyama, K., Awaki, H., Iwasawa, K., & Ward, M. J. 1992, *ApJ*, 399, 129
- Kraft, R. P., Hardcastle, M. J., Worrall, D. M., & Murray, S. S. 2005, *ApJ*, 622, 149
- Leahy, J. P., & Williams, A. G. 1984, *MNRAS*, 210, 929
- Maeda, Y., et al. 2008, *JX-ISAS-SUZAKU-MEMO-2008-06*
- Magdziarz, P., & Zdziarski, A. A. 1995, *MNRAS*, 273, 837
- Magorrian, J., et al. 1998, *AJ*, 115, 2285
- Maiolino, R., Marconi, A., Salvati, M., Risaliti, G., Severgnini, P., Oliva, E., La Franca, F., & Vanzani, L. 2001, *A&A*, 365, 28
- Marchesini, D., Capetti, A., & Celotti, A. 2005, *A&A*, 441, 854
- Marconi, A., & Hunt, L. K. 2003, *ApJ*, 589, 21
- Matsushita, K., Ohashi, T., & Makishima, K. 2000, *PASJ*, 52, 685
- Mitsuda, K., et al. 2007, *PASJ*, 59, S1
- Murphy, K. D., & Yaqoob, T. 2009, *MNRAS*, 397, 1549
- Oosterloo, T. A., Morganti, R., Tzioumis, A., Reynolds, J., King, E., McCulloch, P., & Tsvetanov, Z. 2000, *AJ*, 119, 2085
- Tarchi, A., Brunthaler, A., Henkel, C., Menten, K. M., Braatz, J., & Weiß, A. 2007, *A&A*, 475, 497
- Tueller, J., et al. 2008, *ApJ*, 681, 113
- Ueda, Y., et al. 2007, *ApJ*, 664, L79
- Vasudevan, R. V., Fabian, A. C., Gandhi, P., Winter, L. M., & Mushotzky, R. F. 2010, *MNRAS*, 402, 1081
- Vasudevan, R. V., & Fabian, A. C. 2009, *MNRAS*, 392, 1124
- Vignali, C., Comastri, A., Cappi, M., & Palumbo, G. G. C. 1997, *Mem. Soc. Astron. Italiana*, 68, 139
- Winter, L. M., Mushotzky, R. F., Terashima, Y., & Ueda, Y. 2009, *ApJ*, 701, 1644